Untersuchung der baroklinen Instabilität mittels Infrarot-Thermographie in einem rotierenden differenziell beheizten Ringspalt

Utilizing infrared thermography to investigate baroclinic instability in the differentially heated rotating annulus

Yaraslau Sliavin[1], Peter S. B. Szabo[1], Wolf-Gerrit Früh[2], Björn Schulze[1], Christoph Egbers[1]

[1]Department of Aerodynamics and Fluid Mechanics, BTU Cottbus-Senftenberg, Cottbus, Germany
[2]Ins. Mech., Process and Energy Eng., Heriot-Watt University, Edinburgh, EH14 4AS, UK

Schlagworte: IR-Thermografie, Barokline Instabilität, AtmoFlow
Key words: IR-thermography, Baroclinic instability, AtmoFlow

Abstract

A novel designed differentially heated rotating annulus is used to induce baroclinic waves that are captured by infrared (IR) thermography. The parameter space by this particular experiment provides the possibility of a set of different wave development from regular baroclinic waves to amplitude and structural vacillations. This study will present the investigation of two experiment points (EPs) of well-developed regular baroclinic waves with wave number 3 and 5. The transition to regular wave development is given in a space time plot at the mid gap where the wave number is qualitatively and quantitatively evaluated by a Fast Fourier Transformation (FFT). The general aim for this study is to provide a vast range of baroclinic waves to provide a robust framework to detect baroclinic wave development by a Wollaston Shearing Interferometry (WSI).

Introduction

Planets consist of several layers like an onion such as the inner iron core, the mantel convection or even an atmosphere if present. Today geophysicists and meteorologists are still seeking out to understand the fundamentals of planetary interiors and atmospheres. Anyone who will conduct experiment in a terrestrial laboratory will encounter a challenge – gravity. While gravity increases in the direction from the core to the Earth crust, its magnitude starts decreasing when one moves away from the surface into free space. This radial force field is the main driving force of large-scale thermal transport in the presence of planetary rotation and a temperature difference.

To investigate planetary atmospheres sciences utilise spherical or cylindrical gap geometries that are differentially heated and rotated to study large scale and mesoscale flows such as baroclinic waves experimentally. These simplified models are based on the principle of hydrodynamic similarities to capture such large-scale flows in a miniaturized model that does not lose the overall focus. A differentially rotated baroclinic wave tank (see schematics in Figure 1) was introduced by Hide (1958) and Futz et al. (1959), based on a suggestion of Vettin (1857, 1884). Since then, this particular geometry has been extensively used over several decades to study the main features of large-scale and mesoscale flows, like baroclinic waves

or circulations in planetary atmospheres. This enable to study analogues flow fields that are similar to Earth such as the thermal transport from equatorial to polar latitudes.
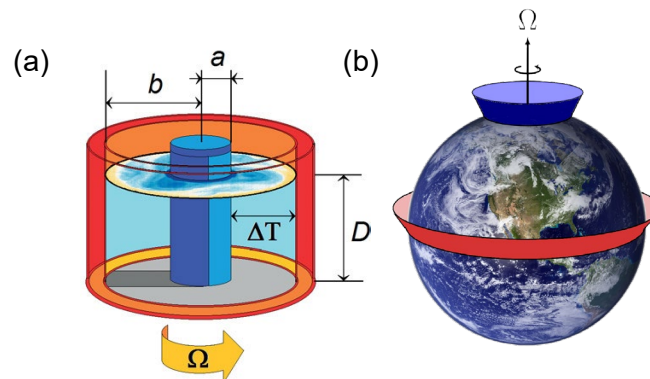

Figure 1: Schematics of a baroclinic annulus in (a) and its analogy to Earth's atmosphere in (b) Vincze (2014) and Rodda (2019).

The aim of this study is to support a spherical gap experiment named AtmoFlow that is used to study planetary atmospheres with an electric central force field to mimic terrestrial gravity (Zaussinger et al. 2019, 2021). The evolving convective flow fields are measured using a Wollaston Shearing Interferometry technique and compared with numerical simulations to reproduce the internal temperature profile (Erdogdu et al. 2021). The validation will be supported by the baroclinic annulus ground-based experiments where the WSI system is benchmarked by IR-thermography to develop methods for the post-processing of recorded interferogram images.

This study will first present the built baroclinic wave tank used to induce baroclinic waves which are captured by IR-thermography. The experiment procedure started first with a benchmark to define the boundaries of the regime diagram of the particular tank where baroclinic waves evolve. This is followed by set of 72 EPs which cover 6 temperature differences and 12 different rotation rates. After conducting all EPs the emerging wave numbers were determined by a spatial spectral analysis. To provide an indication of regular, irregular structural and amplitude vacillations a space time diagram is plotted at the mid-gap of the baroclinic annulus. The results provided are now further utilised to define a parameter space for regular steady wave that will be measured by simultaneous IR-thermography and the WSI system. In the following section the experimental setup is explained in detail.

Experimental setup and experiment procedure

The theoretical experiment setup shown in Figure 2 is built by 3 co-axial aluminium cylinders creating an inner gap, the middle gap and the outer gap. The outer and inner gap are filled with water to establish a temperature difference at the middle gap's boundaries which is the experiment gap filled with the working fluid in which baroclinic waves are induced. The working fluid which is in this case water. Thus, the inner cooled cylinder as shown in Figure 1 (a) presents the polar region and the outer heated cylinder the warmer tropical equatorial region of a planet which is given analogues in Figure 1 (b). The boundary temperatures of the experiment gap are maintained by a thermostat water bath for the inner cylinder that uses a copper heat exchanger to provide a uniform temperature difference at the inner cylinder. To acquire the temperature at the inner gap a 4 lead-wired PT100 sensor is used with an accuracy of ±0.15 K. The outer gap's temperature is maintained by a joule heating wire that is fixed with holders at the outer cylinder and controlled by a self-programmed controller that uses input data of two PT100-sensors to control a power supply of the heating wire. A pump is used and fixed to the outer cylinder to mix the fluid that is heated by the wire to obtain a fairly uniform temperature distribution in the outer cylinder. To evaluate the stability of the installed temperature difference in the system, the second statistical moment the standard deviation, σ, of the temperature is calculated as

$$\sigma = \sqrt{\frac{1}{N-1}\sum_{i=1}^{N}(T_i - \bar{T})^2}. \tag{1}$$

While the time series of the temperature recorded of all sensors were similar to a Gaussian distribution a confidence interval with a probability level of 95% is calculated as ±2σ and was always less than ±0.15 K. A schematic of the experiment setup with the used measurement equipment is given in Figure 2.
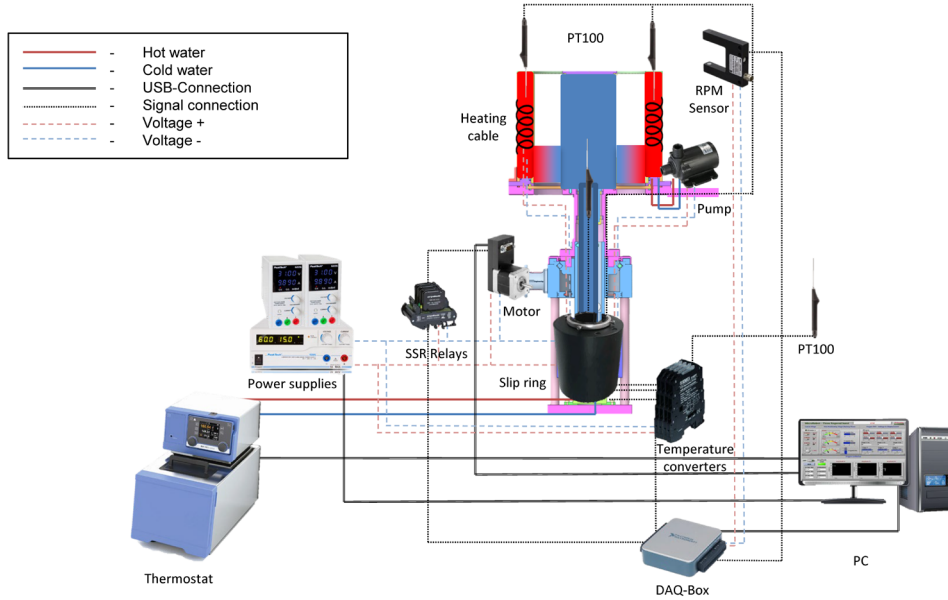

Figure 2: Schematic representation of the experimental setup.

An IR-camera Infratec VarioCam® HD with resolution of 1024x768 px and accuracy of ±1.5 K or ±1.5% is used to record baroclinic wave development at the top surface of the working fluid. The camera's temperature sensitivity at 30°C is given by an accuracy of 0.05 K according to the calibration certification. The IR-data and temperature acquisition was performed by using two program packages, the IRBIS 3 (for IR-Snapshots) and LabView (for temperature and rotation).

To be able to provide a vast parameter range with different aspect ratios the experiment's gap can be filled to different levels to provide a range of aspect ratios. The geometrical parameters and experimental parameter range of the AtmoFlow baroclinic wave tank are found in Table 1. For a non-dimensional characterisation of the baroclinic annulus a parameter space can be evaluated with suitable characteristic numbers suggested by (Früh 1997). One dimensionless number can be formulated by the strength of the Coriolis accelerations and its ratio to viscous dissipation well known as the Taylor number written as

$$Ta = \frac{4\Omega^2(b-a)^5}{\nu^2 D}, \tag{2}$$

where Ω is the angular velocity, ν the kinematic viscosity and a, b and D the geometrical properties of the annulus defined as the inner and outer radii and the fluid depth, respectively. In addition to the Taylor number a second parameter can be formulated as a function of viscous dissipation to Coriolis force known as the Ekman number written as

$$Ek = \frac{\nu}{\Omega D^2}. \tag{3}$$

to define boundary layer thicknesses such as given in Table 1. A third dimensionless parameter may be introduced by a ratio of the strength of the buoyancy forces to the Coriolis force which is captured by the thermal Rossby number and written as

$$Ro = \frac{\alpha \Delta T g D}{\Omega^2 (b-a)^2}, \qquad (4)$$

where g is the gravitational acceleration and α the thermal expansion coefficient. When the temperature, rotation rate or aspect ratio is changed, one can define a parameter space in the Taylor-Rossby space for flow regimes that suggest axisymmetric, regular waves or irregular, periodic structures such as amplitude or structural vacillations as is displayed in Figure 3. This regime diagram is used to quantify the evaluated results for the AtmoFlow wave tank and to define the EPs that are evaluated in the experiment plan.

Table 1: Geometrical and experimental parameter range of AtmoFlow baroclinic wave tank.

Geometric dimensions			
Inner radius	a	mm	100
Outer radius	b	mm	200
Gap width	$L = b - a$	mm	100
Fluid depth	D	mm	$25 - 150$
Aspect ratio	$\Gamma = L/D$	–	$0.67 - 4$
Experiment conditions			
Temperature inner wall	T_C	°C	11
Temperature outer wall	T_H	°C	40
Temperature difference	$\Delta T = T_H - T_C$	K	$0 - 25$
Rotation rate	f_0	rpm	$0 - 25$
Ekman layer thickness	$\delta_E = D E k^{1/2}$	m	$0 - 0.0078$
Stewartson layer thickness	$\delta_S = (b-a) E k^{1/3}$	m	$0 - 0.0458$
Thermal layer thickness	$\delta_T = D \left(\dfrac{\nu k}{g \alpha \Delta T L^3} \right)^{1/4}$	m	$0 - 0.0012$
Fluid properties			
Density	ρ	kg m⁻³	998.21
Kinematic viscosity	ν	m² s⁻¹	1.004×10^{-6}
Thermal diffusivity	k	m² s⁻¹	0.1434×10^{-6}
Volumetric expansion coefficient	α	K⁻¹	0.207×10^{-3}
Prandtl number	Pr	–	7
Azimuthal wavenumber	m	–	$3 - 7$

Image post treatment and data processing

The recorded surface temperature by the IR-camera is stored in a cartesian grid. The values are post treated by masking the experiment gap where all other values are changed to NAN. The mask is generated by triangulation. While the IR-camera is not co-rotating with the baroclinic tank's angular velocity, the rotation needs to be subtracted such that the observation of baroclinic wave development can be evaluated in the rotating frame of reference. The temperature transformation to the rotating frame of reference is performed for each EP's angular velocity with the respect to the camera's frame rate. The resulting temperature profile is then plotted in contours by normalizing the temperature with

$$T' = \frac{T - T_C}{T_H - T_C}. \qquad (5)$$

To evaluate the evolving temperature in space time Hovmöller diagrams are used by plotting the temperature at the mid-gap in azimuthal direction versus time (Hovmöller 1949). The time is normalized by the angular velocity written as

$$t' = \Omega t. \tag{6}$$

A spatial FFT is used to evaluate the wave number at the mid-gap for the last timestep and over the complete time at a fixed point, $\varphi = 0$.
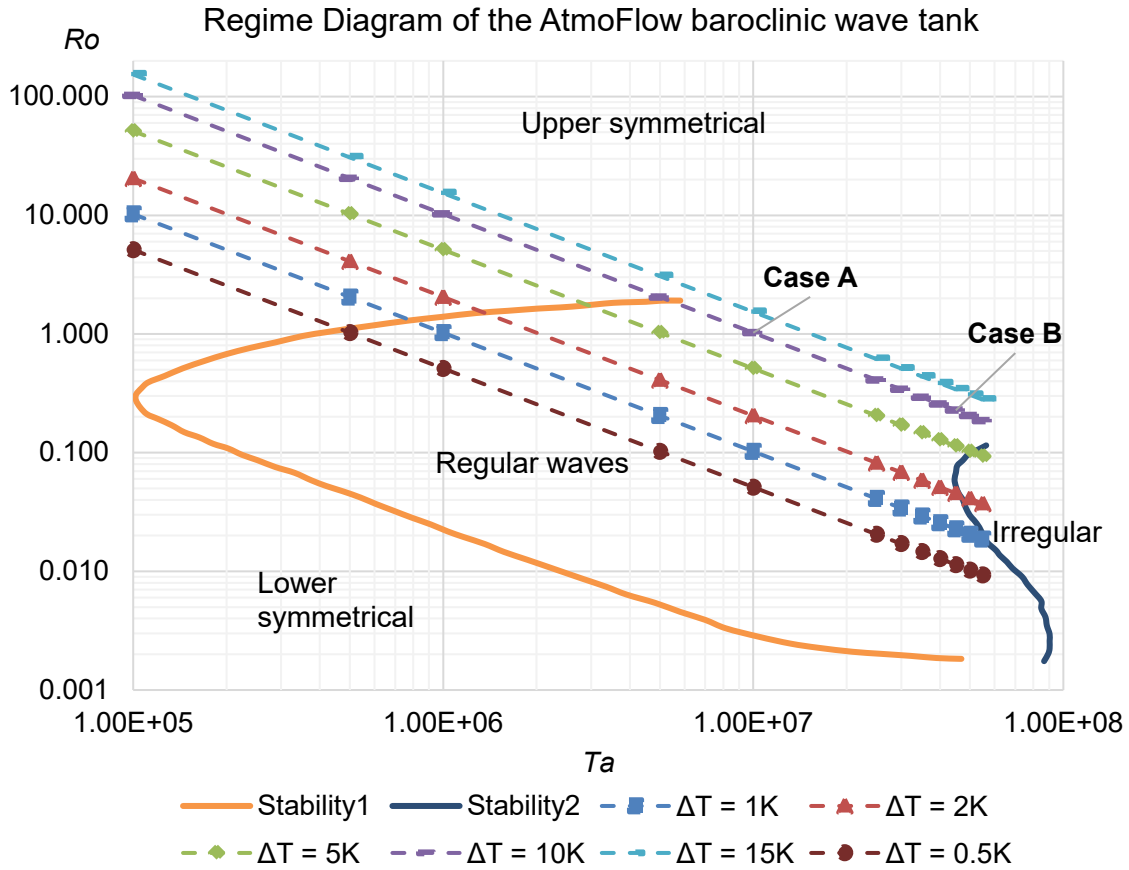

Figure 3: Estimated regime diagram for the AtmoFlow baroclinic wave tank of the first measurement campaign by using the Taylor-Rossby space.

Results and discussion

(a)
$Ro = 1.02$ and $Ta = 1.0 \cdot 10^7$
$\Delta T = 10K$ and $f = 6.06$ rpm

(b)
$Ro = 0.23$ and $Ta = 4.5 \cdot 10^7$
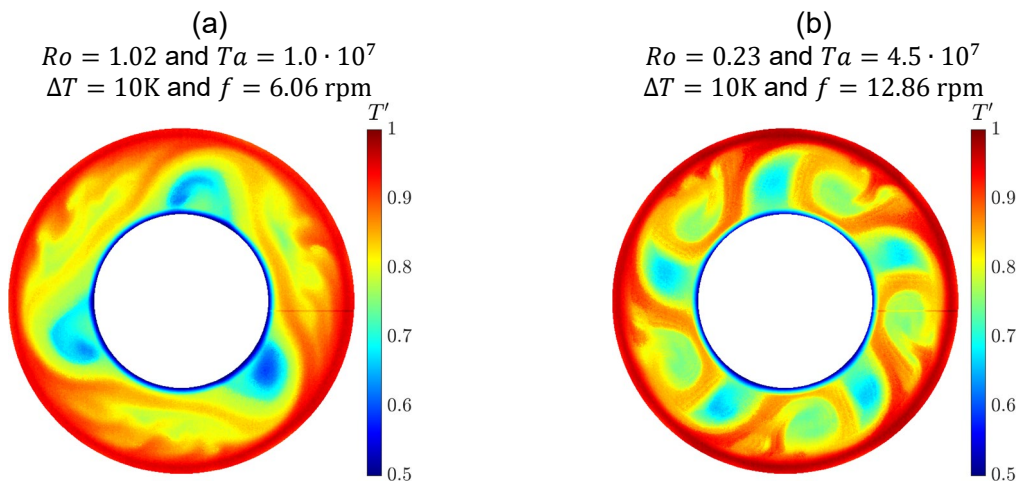$\Delta T = 10K$ and $f = 12.86$ rpm

Figure 4: Contour plot of normalized temperature, T', of the last image frame in the left panel (a) with wave number 3 and right panel (b) with wave number 5 for the EP cases (A) and (B), respectively.

In total 72 EPs were recorded to benchmark the AtmoFlow wave tank and to evaluate different baroclinic wave development that may be relevant to the AtmoFlow space experiment. During the complete measurement campaign several different flow regimes are obtained with wave numbers starting from $n = 3$ to 7 with regular, amplitude vacillations, structural, vacillations and irregular waves were found. Here, we only present the regular wave development of two EPs defined as case (A) and case (B) which are shown in Figure 4 (a) and (b), respectively. The recorded surface temperature profiles indicate well developed regular baroclinic waves with wave number $n = 3$ and $n = 5$. When Ta is increased, anvil shaped structures of thermal plumes appear that are indicative for case (B) compare to case (A).

A time resolved Hovmöller diagram in Figure 5 (a) at the mid-gap provides the time evolution of the baroclinic wave that captures the onset and transition from an axisymmetric regime to the stable wave development for case (A). The transition up to a stable regular wave number $n = 3$ takes for this particular case (A) about $t' = 250$. However, even here the regular wave structure appears to have some structural changes over time with respect to plumes detaching from the tangent cylinder.
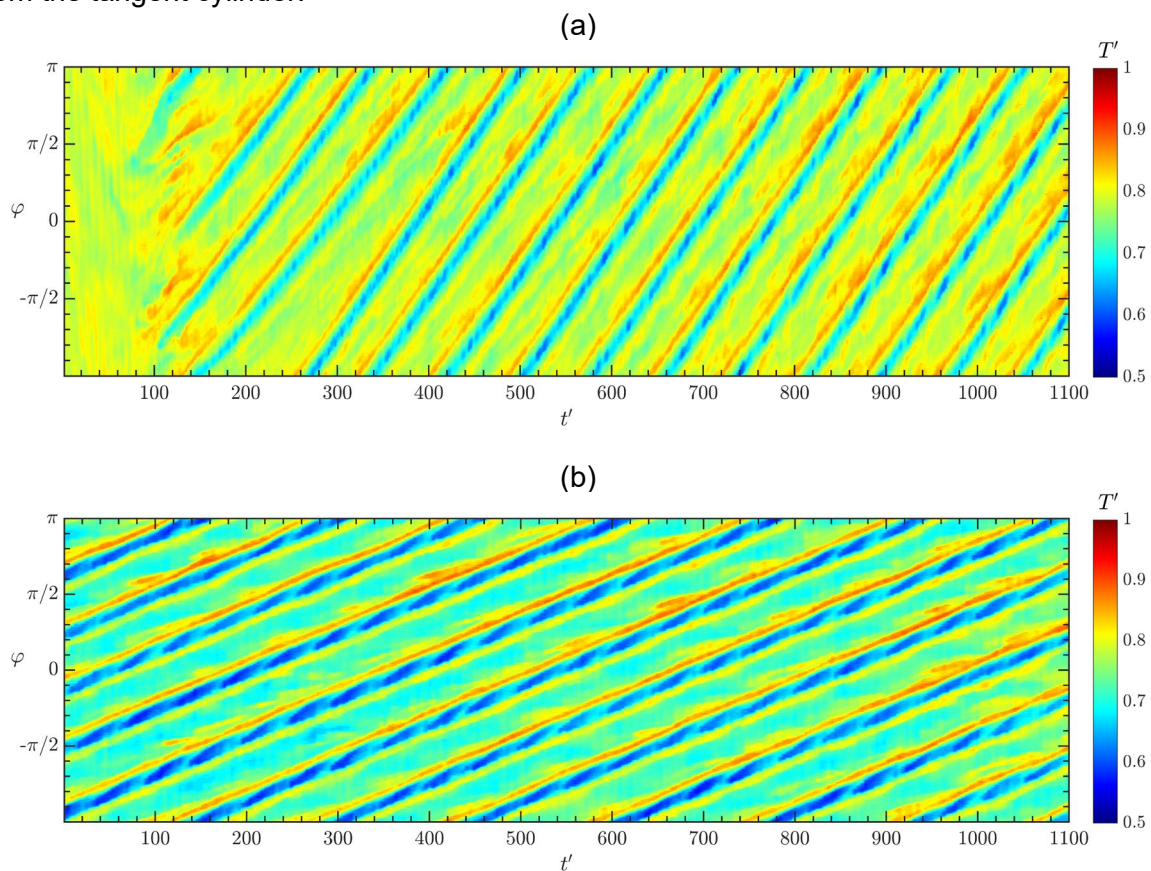
(a)

(b)

Figure 5: Contour plot of normalized temperature, T', at mid-gap plotted versus the normalized time t' for case (A) and (B) in the upper and lower panel (a) and (b), respectively. Note, that the time t' starts in the upper panel prior to wave development whereas the lower panel starts after the baroclinic waves are fully developed.

This is also observed for case (B) displayed in Figure 5 (b). The Hovmöller diagram shows a clear baroclinic wave number $n = 5$ through the complete time evolution after the wave had clearly settled. However, the plot indicates clear detached hot zones from the regular shape that seem to repeat over time in similar shape form the anvil-shaped structures that are indicative as seen in Figure 4 (b). Considering this regular wave pattern one can identify the onset of amplitude vacillations with small structural changes of some detached thermal zones from the tangent cylinder where the transition may be close to start irregular waves if the Taylor number is increased. Nevertheless, the two investigated cases could still be referred as regular waves despite the occurrence of small structural changes and amplitude vacillations.

Comparing both time wave evolutions in Figure 5 with one another one can clearly identify a drift speed of the baroclinic waves in the rotating frame of reference through the annulus in azimuthal direction. The drift time can be determined for case (A) to about $t' = 245$ and for case (B) about $t' = 146$.

The wave number, n, of the observed baroclinic waves in both cases may also be quantitatively evaluated by a spatial FFT and is performed for the last time step at the mid-gap and presented in Figure 6. In case (A) strong amplitudes are seen at $n = 3$ and 6 are observed suggesting a dominate wave number $n = 3$. However, this is different to case (B) where a strong wave number $n = 10, 5, 15$ and 20 are observed suggesting a wave number 10. While a qualitative observation of Figure 4 (b) suggests more like a wave number 5, it can be interpreted by a separation effect of the anvil-shaped structures by hot jets from the outer to the inner cylinder suggesting a wave number 10.
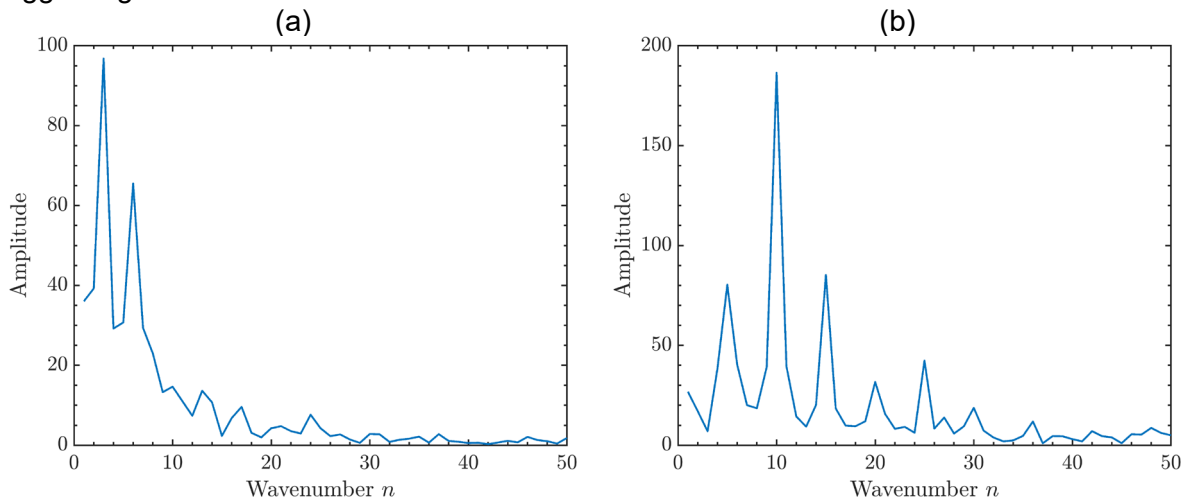

Figure 6: Spatial FFT over the mid-gap for case (A) and (B) in the left and right panel, respectively.

A second FFT can be used to analyze the wave development at a fixed position e.g. at the mid-gap at $\varphi = 0$ and is plotted in Figure 7. Case (A) shows a clear peak at ~ 0.0126 and its harmonic typical for a steadily progressing steady wave. In contrast, the case (B) has a broader feature around 0.006 in addition to clear peaks at around 0.012 and 0.018. This spectrum indicates to onset of a modulation of the wave almost but not fully commensurate with its progression through the annular channel.
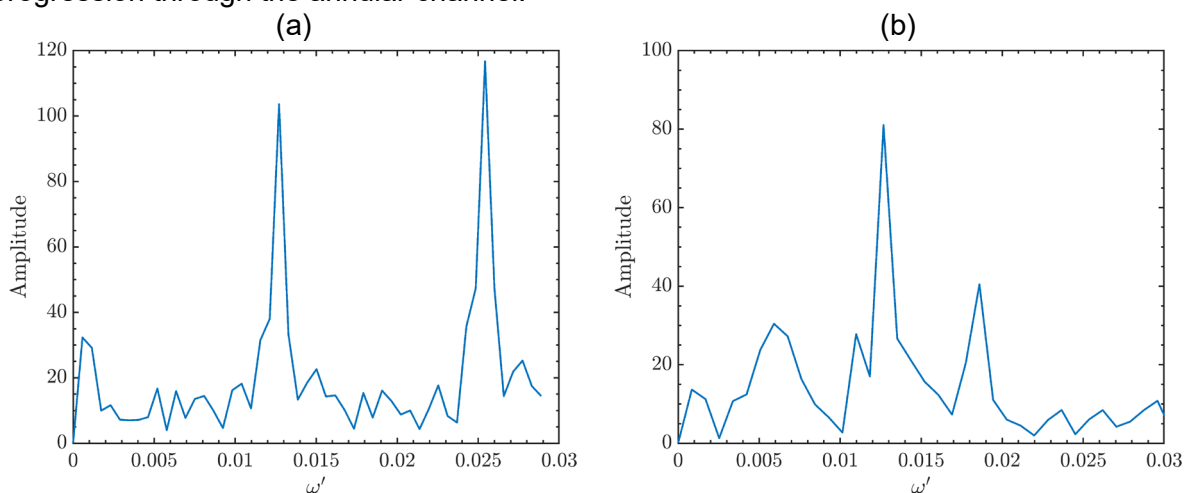

Figure 7: Temporal FFT at mid-gap over a fixed point $\varphi = 0$ for case (A) and (B) in the left and right panel, respectively.

Conclusions

In this study baroclinic instability in the rotating differentially heated annulus is investigated with open top surface to utilise IR-thermography. The technique provided a robust visualisation of baroclinic wave and their spatial and structural development. In total 72 EPs are recorded whereas two EPs of regular baroclinic waves with wave number 3 and 5 were investigated. To visualise the onset and regular wave development Hovmöller diagrams are used to plot the azimuthal mid-gap temperature in time at the mid-gap. This provides a clear understanding of regular wave development for both EPs. A spatial FFT was used at to quantified the wave number at last time-step where a second FFT was investigating the wave development at the fixed point $\varphi = 0$ both at the mid-gap. Further investigation for the other recorded FFTs are still pending and will be used to filter most dominant wave structures to recreate temperature fields by an inverse FFT. This may provide a possibility to understand irregular wave development of baroclinic wave prior to conduct more complex evaluations such as principal component analysis or dynamic mode decomposition. To summarize, this study provided regular baroclinic wave development in the AtmoFlow wave as a benchmark tank which suggests a robust framework to use novel experimental technique the Wollaston Shearing interferometry for further investigations.

Acknowledgement

References

Erdogu, A.O., Szabo, P.S.B, Carter, R., Gevrek, M.-E., Haun, P., Zaussinger, F., Schulze, B., Meier, M., Egbers, C., 2021: Utilizing Wollaston shearing interferometry to investigate the refractive index gradient in a differentially heated annulus. – Fachtagung "Experimentelle Strömungsmechanik"

Fultz, D., Long, R. R., Owens, G. V., Bohan, W., Kaylor, R., and Weil, J., 1959: Studies of thermal convection in a rotating cylinder with some implications for large-scale atmospheric motions, Meteor.

Früh W-G., 2015: Amplitude vacillation in baroclinic flows. In von Larcher T, Williams PD, editors, Modelling Atmospheric and Oceanic Flow: Insights from laboratory experiments and numerical simulations. Wiley. 61-81.

Früh W. G., Read P. L.,1997: Wave interactions and the transition to chaos of baroclinic waves in a thermally driven rotating annulus Phil. Trans. R. Soc. A.355101–153

Hide, R., 1958: An experimental study of thermal convection in a rotating fluid, Phil. Trans. Roy. Soc. Lond. A, 250, 441–478.

Hovmöller E., 1949: The Trough-and-Ridge diagram. Tellus. 1. 62 - 66.

Rodda C., 2019: Gravity wave emission from jet systems in the differentially heated rotating annulus experiment**,** Cuvillier Verlag, Göttingen, 200.

Vettin, F., 1857: Uber den aufsteigen Luftström, die Entstehungdes Hagels und derWirbel-Stürme, Ann. Physik Chemie, 102, 246–255.

Vettin, F., 1884: Experimentale Darstellung von Luftbewegungen unter dem Einflusse von temperatur-unterschieden und rotations-impulsen, Meteorolol. Z., 1, 227–230, 271– 276.

Vincze, M., S. Borchert, U. Achatz, T. von Larcher, M. Baumann, C. Hertel, S. Remmler, T. Beck, K. Alexandrov, C. Egbers, J. Fröhlich, V. Heuveline, S. Hickel, U. Harlander, 2014: Benchmarking in a rotating annulus: a comparative experimental and numerical study of baroclinic wave dynamics. – Meteorol. Z. 23, 611–635.

Zaussinger, F., Canfield, P., Froitzheim, A., Travnikov, V., Haun, P., Meier, M., ... & Egbers, C.,2019: AtmoFlow-investigation of atmospheric-like fluid flows under microgravity conditions. Microgravity Science and Technology, 31(5), 569-587.

Zaussinger, F., Haun, P., Szabo, P. S., Travnikov, V., Al Kawwas, M., & Egbers, C., 2020: Rotating spherical gap convection in the GeoFlow International Space Station (ISS) experiment. Physical Review Fluids, 5(6), 063502.